A RECONSTRUCTION ALGORITHM FOR THREE DIMENSIONAL ELECTRICAL IMPEDANCE TOMOGRAPHY

G. A. Kyriacou*, C.S. Koukourlis*, P. Bonovas* and John N. Sahalos**

*Department of Electrical and Computer Engineering, Demokritos University of Thrace
**Department of physics, Aristotle University of Thessaloniki
Microwaves Lab., GR-67 100 XANTHI, GREECE
E-mail : gkyriac@xanthi.cc.duth.gr

Abstract

A reconstruction algorithm for three-dimensional (3-D) Electrical Impedance Tomography is developed based on the extension of the modified perturbation method. For this purpose the forward problem is solved by using the finite element method (FEM). Also, the partial derivatives of the surface voltages with respect to conductivity (Jacobian matrix) are given in closed form expressions. The selection of driven electrode pairs and the data collection schemes are examined. The validity and the performance of the proposed algorithm is tested and some successfully reconstructed 3-D computer phantoms are presented.

1. INTRODUCTION

The reconstruction of the conductivity (or resistivity) distribution of an object through low frequency electrical measurements is known as Electrical Impedance Tomography (EIT). EIT is a new non-ionizing and non-invasive imaging technique with widespread applications especially in medicine, [1], and geophysical prospecting, e.g. [2, 3, 4]. The major differences in these two applications are related to the measurement or data collection system, while the same reconstruction algorithm can be employed in both cases. Let us restrict ourselves in the medical applications which are of particular interest in general. EIT imaging is established on the fact that biological tissues can be recognized from their conductivity (σ) and permittivity (ε). Since, the tissue electrical properties vary according to the state of health as well as during physiological organs functioning, it is then evident that E.I.T. can be used for medical diagnosis and dynamic events monitoring purposes respectively.

In order to extract the necessary information about the conductivity distribution to be sought, arrays of electrodes are attached on the surface of the body under test. A series of low frequency sinusoidal current patterns (usually between 10 and 100 kHz) are injected. Each pattern is applied through a different subset of "active" electrodes (usually just two) and the voltage developed on all the other electrodes-sensors is measured. Frequencies

lower than 10 Hz are absolutely prohibited to avoid electrolysis effects at the electrode/tissue interface and ion migration (iontophoresis) effects. In fact frequencies greater than 10 kHz are recommended in order to safely avoid interference from the internal bioelctric sources. Also, the magnitude of the applied current density must be less than 10mA/cm^2 for safety reasons, [5].

The aim of EIT is to use the measured voltage data set to extract the object's conductivity distribution. This is basically an inverse electromagnetic problem, which turns out to be a strongly non-linear one. Even worst, this inverse problem is also an ill-conditioned one in general. The ill-conditioning is due to the basic fact that the electric current spreads out as we move away from the electrode, leading to curved current streamlines or curved equipotential lines, which are also more dense near the electrode than away from it. Moreover, the current streamlines (equipotential lines) depend on the conductivity distribution itself justifying the inverse problem non-linearity. The current spreading extends to the third dimension as well making the inverse problem a strictly three-dimensional (3-D) one. In other words the electric current cannot be constrained to flow in a plane, even when coplanar active electrodes are employed. It is deeply spread above and below the active electrodes plane. Also, the conductivity distributions of practical interest are mostly 3-D. Even though, the majority of reconstruction algorithms used in EIT assumes a two-dimensional (2-D) domain and there was only a little effort toward the 3-D imaging, [5, 7-11]. This is logical and it was expected since an essential solution to the problem should be obtained first. Moreover, there is some evidence, [12], that the employment of 3-D modelling and reconstruction will made calculations more compatible with measurements and reduce the ill-conditioning. This is mainly due to the fact that measurements are carried out on a real 3-D object which is obviously better described by a 3-D computer model. It is now well understood that EIT imaging must move-on toward 3-D and try to satisfactorily face the complexity involved in the corresponding reconstruction algorithms.

As explained above, EIT is a nonlinear and generally ill-posed 3-D inverse problem. Due to its non-linearity this problem cannot be solved in a single iteration. An initial conductivity estimation (starting solution) is assumed and the problem is directly (or indirectly) linearized and solved about it to obtain an improved solution. The procedure is iteratively repeated until a reasonable image is obtained. During each iteration, the forward problem (Laplace equation) is solved on a computer model. Using the FEM, the

object is discretized into homogeneous volume elements (voxels), namely a piecewise constant distribution. At each solution, the voltage at the points corresponding to the measuring electrodes are calculated. A vector of voltage differences between measurements and calculations is formed and used to update the conductivity. The procedure stops when the mean square difference between calculations and measurements approaches the measurements error.

Let us now briefly describe some of the existing 3-D EIT reconstruction algorithms in order to point out the necessity for further investigation. Wexler et al [3, 7] developed their algorithm, called "double constrained" method, for both 2-D and 3-D imaging. It's main advantage is the stability and the disadvantage is the slow rate of convergence. Kotre [8], proposed a 3-D reconstruction algorithm based on a sensitivity matrix (change of a voltage difference with respect to a change of an element's conductivity). The calculation of this matrix seems to be very time consuming, especially if it is to be calculated for each conductivity profile in a possible iterative approach. Liu et al [9], employed the Newton Raphson technique [6] for a 3-D model of 3x4x4 voxels and they suggested that the diagonal placement of active electrodes better discriminates conductivity variations while coplanar electrodes performed better when the target conductivity was of a 2-D nature. Newton-Raphson involves multiple matrix inversion and suffers from matrix ill-conditioning. The purpose here is the development of a fast iterative 3-D reconstruction algorithm avoiding matrix inversions and the related ill-conditioning.

Working toward the above purpose, we have extended the 2-D Modified Perturbation Method (MPM), [12], for a 3-D reconstruction. The first attempts to reconstruct 3-D computer phantoms were presented in [10] but various difficulties were faced when the target conductivity profile was inhomogeneous in all three-dimensions. These problems were latter clarified and inhomogeneous 3-D computer phantoms were successfully reconstructed, especially by the proper selection of projection angles (active electrode pair positioning). A presentation of this work is to be tried herein.

Since, the inverse problem involves multiple solutions of the forward problem, let us first describe the FEM solution employed for this purpose.

2. THE FORWARD PROBLEM - FEM SOLUTION

The forward problem involves the injection of a sinusoidal current pattern with the aid of a number of electrodes and the calculation of the potential distribution over the object volume. The problem is generally governed by Maxwell equations restricted to the low frequency (f<100KHz) case where a "quasi-static" condition is valid. This is reasonable, since the wavelength (λ) at these frequencies is quite larger than the object dimensions. Thus the propagation effects can be neglected, but even more the field intensities (or the potential) can be considered to vary synchronously with time over the whole object. Keeping in mind that the conductivity distributions of practical interest are inhomogeneous, the forward problem is reduced to the generalized Laplace or Poisson equation. Furthermore, the materials to be studied, like the biological tissues, exhibit high dielectric constants. This in general can be accounted by introducing the complex dielectric constant, as $\varepsilon_r^* = \varepsilon_0\varepsilon_r[1-j(\sigma/\omega\varepsilon_0\varepsilon_r)] = \varepsilon_0\varepsilon_r\,(1-j\tan\delta)$, were $\tan\delta$ is the loss tangent. This will result in a complex voltage distribution $\overline{V}$, where the real part (V_r) is "in-phase" with the excitation current and depends on the conductivity, while its imaginary part (V_i) is "out-of-phase" and depends on the permittivity distribution. These two voltage components are measured separately (by synchronous demodulation) and can be used for the reconstruction of the conductivity and permittivity distributions correspondingly. The forward problem equations can be written as :

$$\overline{\nabla}\bullet(\overline{\overline{\varepsilon}}\,\overline{\nabla}V_i) = -\rho \quad \text{or} \quad \iiint_{V_\delta}\left\{\frac{\partial}{\partial x}\left(\varepsilon_x\frac{\partial V}{\partial x}\right)+\frac{\partial}{\partial y}\left(\varepsilon_y\frac{\partial V}{\partial y}\right)+\frac{\partial}{\partial z}\left(\varepsilon_z\frac{\partial V}{\partial z}\right)\right\}dV_\delta = -\iiint_{V_\delta}\rho\, dV_\delta \tag{1}$$

$$\overline{\nabla}\bullet(\overline{\overline{\sigma}}\,\overline{\nabla}V) = \frac{\partial\rho}{\partial t} \quad \text{or} \quad \iiint_{V_\delta}\left\{\frac{\partial}{\partial x}\left(\sigma_x\frac{\partial V}{\partial x}\right)+\frac{\partial}{\partial y}\left(\sigma_y\frac{\partial V}{\partial y}\right)+\frac{\partial}{\partial z}\left(\sigma_z\frac{\partial V}{\partial z}\right)\right\}dV_\delta = -\oiint_{S}\overline{J}\cdot d\overline{S} \tag{2}$$

where S is a closed surface bounding the volume V_δ of the object. The current ($\overline{J}$) and charge (ρ) densities represent the internal sources, which are set to zero since they do not exist in the EIT case. In the general FEM solutions, the object can be considered to be described by diagonal anisotropic tensors $\overline{\overline{\sigma}}=(\sigma_x, \sigma_y, \sigma_z)$, $\overline{\overline{\varepsilon}}=(\varepsilon_x, \varepsilon_y, \varepsilon_z)$ defined by the conductivities and permittivities along the x, y, z axes. In this case EIT algorithms should be used for three times more unknowns. When the internal sources vanish (J=0, ρ=0), Eqs.(1) and (2) become exactly similar, each one involving a pair of variables ($\overline{\overline{\sigma}}$, V_r) and

($\bar{\bar{a}}$, V_i). It is then expected that the same algorithm developed for the reconstruction of conductivity (σ) from the "in-phase" voltage distribution (V_r), can be used to reconstruct permittivity (ε) from the "out-of-phase" voltage distribution (V_i). In the present case, we restrict ourselves to the isotropic ($\sigma_x=\sigma_y=\sigma_z=\sigma$) homogeneous case and to the "in-phase" voltage distribution (symbolized just as V from now on), namely only the conductivity distribution will be sought.

The Finite Element Method (FEM) is widely used for the solution of partial differential equations like (1) or (2) and especially within inverse problems, because FEM is more compatible with them. The volume is divided into small homogeneous elements (voxels) with conductivity σ_j (piecewise constant distribution). The voltage distribution is also discretized and is to be calculated at certain points called "nodes" which usually coincide with the element vertices. These elements as well as their nodes are uniquely numbered for the whole solution domain and this is defined as "global element/node numbering". The excitation current is introduced through the Neumann boundary conditions, as :

$$-\sigma \frac{\partial V}{\partial n} = \begin{cases} J & \text{on the electrodes} \\ 0 & \text{at the body} - \text{air interface} \end{cases} \tag{3}$$

where $\partial V/\partial n$ is the potential derivative normal to the surface. Eq.(2) is also subjected to a mixed Dirichlet and Neumann (or impedance) boundary condition which is intrinsically imposed at the interface between different elements.

$$V_i = V_j \quad \text{and} \quad \sigma_i \frac{\partial V}{\partial n_i} = \sigma_j \frac{\partial V}{\partial n_j} \tag{4}$$

With the aid of the variational technique, Eq.(2) along with the above boundary conditions is reduced to the minimization of the following functional :

$$F(V) = \frac{1}{2} \iiint_V \left\{ \sigma_x \left(\frac{\partial V}{\partial x}\right)^2 + \sigma_y \left(\frac{\partial V}{\partial y}\right)^2 + \sigma_z \left(\frac{\partial V}{\partial z}\right)^2 \right\} dxdydz + \oiint_S JVdS \tag{5}$$

S is a closed surface bounding the solution volume V which is actually reduced to the surface of the current carrying electrodes. In order for F(V) to be minimized, its partial derivatives with respect to the nodal voltages (V_i) should be set to zero :

$$\frac{\partial F(V)}{\partial V_i} = 0 \qquad \text{for } i = 1, 2, \ldots . Np \tag{6}$$

where Np is the number of nodes.

Instead of integrating (5) over the whole domain, it can be integrated over each element separately. For this purpose an arbitrary interpolation function $V^e(x, y)$, usually of a polynomial form, is assumed for the potential. Its number of unknowns must be equal to the element's degrees of freedom, which in this case is the same as the number of nodes. Eight nodes parallelepiped elements (Fig.1) and a trillinear interpolation functions is considered as :

$$\left.\begin{aligned} V^e(x,y,z)&=(a_1+a_2x)(b_1+b_2x)(c_1+c_2x) \\ \text{or } V^e(x,y,z)&=g_1+g_2x+g_3y+g_4z+g_5xy+g_6xz+g_7yz+g_8xyz \end{aligned}\right\} \quad (7)$$

g_i can be removed by expressing them as a function of the nodal voltages.

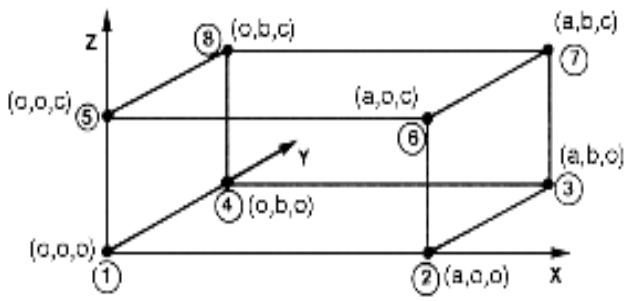

Figure 1. An eight node parallelepiped element with its local coordinates.

This can be simply done by applying equation (7) on each node of the element with the "local" coordinates appearing in Fig.1. This can be done for just one element, because all elements of the solution domain are similar. Solving the resulting system of the eight equations and substituting into Eq.(7) one gets :

$$V^e(x,y,z)=\frac{1}{\ddot{A}}\sum_{i=1}^{8} f_i(x,y,z)V_i \quad (8)$$

where : Δ=abc the volume of the element and a, b, c its dimensions and

$f_1=(a-x)(b-y)(c-z)$, $f_2=x(b-y)(c-z)$, $f_3=xy(c-z)$, $f_4=(a-x)y(c-z)$,

$f_5=(a-x)(b-y)z$, $f_6=x(b-y)z$, $f_7=xyz$, $f_8=(a-x)yz$.

The interpolation function V^e is introduced in Eqs.(6) and (5) in turn and the differentiations and integrations involved therein are analytically carried out. Any excitation current injected through the nodes of the element are introduced through the second term of Eq.(5). If there is not any injected current at some node then this term is

just set to zero. This process results in a system relating the element nodal voltages (vector $[V]^e$) with the nodal excitation currents vector $[I]^e$ through the element admittance matrix $[Y]^e$, as :

$$[Y]^e [V]^e = [I]^e \tag{9}$$

For the parallelepiped element the element admittance matrix can be expressed as :

$$[Y]_8^e = \frac{\acute{o}_j}{2\ddot{A}} \begin{bmatrix} G_1 & G_2 & G_3 & G_4 & G_5 & G_6 & G_7 & G_8 \\ & G_1 & G_4 & G_3 & G_6 & G_5 & G_8 & G_7 \\ & & G_1 & G_2 & G_7 & G_8 & G_5 & G_6 \\ & & & G_1 & G_8 & G_7 & G_6 & G_5 \\ & & & & G_1 & G_2 & G_3 & G_4 \\ & & & & & G_1 & G_4 & G_3 \\ & & & & & & G_1 & G_2 \\ \text{symmetric} & & & & & & & G_1 \end{bmatrix} \tag{10}$$

where $G_1 = 4D + 4E + 4F$, $G_2 = -4D + 2E + 2F$, $G_3 = -2D - 2E + F$,

$G_4 = 2D - 4E + 2F$, $G_5 = 2D + 2E - 4F$, $G_6 = -2D + E - 2F$,

$G_7 = -D - E - F$, $G_8 = D - 2E - 2F$,

$D = b^2c^2$, $E = a^2c^2$, $F = a^2b^2$

In system (9) each equation represents one node of the element, but in the whole solution domain each node may belong to more elements, from one to at max eight as shown in Fig.2b. Thus, there may be up to eight equations for the same node. These can be added together to give a unique equation for each node which contains all the contributions to this node. This procedure is known as "master matrix assembly" and leads to a system of equations for all the nodal voltages and currents of the solution domains as :

$$[Y] [V] = [I] \tag{11}$$

where [Y] is the admittance matrix of the structure.

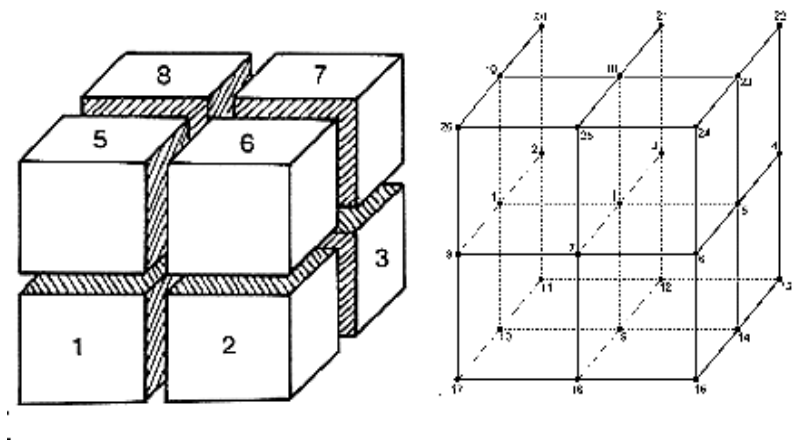

a b

Figure 2. Neighboring elements and nodes of an arbitrary ith node, a) The 27 neighboring nodes and their local numbering and b) The 8 neighboring elements and their local numbering.

An important feature can be seen in Fig.2b where each node-i has only up to 27 neighboring nodes including itself. Also, the 8-elements around it can relate its nodal voltage only to these 27 nodal voltages. This means that there are only up to 27 nonzero entries in each line (equation) of matrix [Y] in Eq.(11). A very efficient master matrix assembly technique has been proposed by Kim [13] and employed herein, based on this observation. The ordinary procedure, which is also the only one possible for arbitrary shaped elements, is to calculate the element matrix $[Y]^e$ and add its coefficients into the proper positions (denoted by the global node numbering) in the matrix [Y]. Scanning in this manner all the elements we result in the assembly of the matrix [Y]. For simple geometrical elements, like the parallelepipeds, it is easy to locate (mathematically) the global node numbers. Equivalently, the global numbers of the 27 locally numbered nodes in Fig.2a are estimated by virtually putting it over the whole domain so that the ith node coincides with the desired global one. Then, according to Kim [13], instead of scanning the elements we scan the nodes of the global domain for the master matrix assembly. So, the eight equations for the ith node are added together or their contributions to the 27 non-zero coefficients are directly estimated. In this manner, there is no need to store a Y(NpxNp) real matrix but only a Y(Npx27) real master matrix an a NEBOR (Npx26) integer matrix containing the global numbers of the 26 neighbors of each ith node. This storage results in a reduction of the order of Np/40 (Np = total number of nodes) of the memory requirements, [13]. The resulting system of equations is solved by using the Gauss-Seidel iterative scheme modified by Kim [13] to include a relaxation factor k. Each nodal voltage is updated according to the following formulae :

$$\left.\begin{aligned} V_i^n &= V_i^{n-1} + k \cdot \left(\hat{V}_i^n - V_i^{n-1}\right) \\ \hat{V}_i^n &= \left\{ I_i - \sum_{\ell=1}^{26} Y_{i\ell} V_\ell^m \right\} \Big/ Y_{i1} \end{aligned}\right\} \tag{12}$$

ℓ = NEBOR(j, i) = global number of the jth neighboring node to the ith node-line currently processed. Y_{i1} is the coefficient of V_i itself and V_ℓ^m the voltage of the ℓth node, some of which are updated at the current (n) and some in the previous (n-1) iteration. The algorithm starts from an initial solution $[V]^o$ and all nodal voltages are

updated at each iteration. This is iteratively repeated until the maximum voltage change, (error) at any node, between successive iterations becomes less than a prespecified error tolerance (e.g. 10^{-6}). The relaxation factor value is in general between 0 and 2. For the solution of Laplace equation we found that the optimum value giving the fastest convergence is k=1.75. It is also important to note that the boundary conditions imposed above do not include any rigid one, since the excitation current sources considered define only the derivative of the potential ($\partial V/\partial n$). Thus, the resulting potential distribution is floating, because there are multiple solutions different only by an additive constant. Mathematically, this situation results in a non-full rank matrix Y (its rank is Np-1). This problem can be solved by providing a reference node for the potential distribution. Usually a zero potential is assumed for this node because it is virtually grounded. For direct techniques all the coefficients of the corresponding line are set to zero except the diagonal one which can be set to one while the right hand side (current applied to this node) is also set to zero. Moreover, the reference node in EIT should not be a peripheral one, because it may cause convergence problems.

There is some evidence, [14], that a direct technique like the LU decomposition should be used for the solution of FEM systems within EIT. This is because the system [Y][V]=[I] is solved for multiple injection current patterns [I] with the same matrix [Y]. Thus the decomposition of matrix [Y] into an Upper and a Lower one (L, U) needs to be done only once within each iteration. This is actually true for a small number of nodes, as for example in 2-D models. But, it is questionable as the number of nodes is increased (as in 3-D models). Moreover, it has been proved, [14], that the required CPU time is proportional to $\propto Np^3$ for direct methods like Gauss elimination or LU decomposition and is reduced to $\propto Np^{1.85}$ when sophisticated node numbering is employed (to reduce the band of the matrix [Y]) in conjunction with the best sparse matrix method. While, it has been proved in our previous work [15] as well as by Jorgenson et al [16], that the CPU time requirements of the Gauss-Seidel technique is just linearly proportional to the number of nodes ($\propto N$). Furthermore, in iterative techniques a voltage distribution obtained for a specific excitation current pattern (projection angle) is stored in memory and it is then used as an initial guess for the same projection angle in the next EIT iteration. In this manner the Gauss-Seidel is drastically speed up and needs about the half number of iterations to achieve convergence.

3. RECONSTRUCTION ALGORITHM

As explained in the introduction in order to reconstruct the conductivity distribution of an object, arrays of electrodes are placed on its surface which are uniformly distributed over it. A sinusoidal current pattern is applied through a subset of these electrodes and the voltage developed on all the others is measured. In this work we consider excitation by a single current generator or that just a pair of active electrodes is used to inject current. The active electrodes pair is in turn rotated/moved about the surface of the object and the voltage measurements are repeated to collect the total vector (V_m). To collect a similar set of calculated voltages (V_c), a FEM model describing the real object as close as possible is constructed. If any a priori information about the object conductivity distribution is known, then it is used in the initial guess, otherwise a homogeneous starting model is assumed. A similar series of excitations as that used in measurements is applied and for each one the generalized Laplace equation is solved to calculate the voltages at the electrode positions. The differences between the measured and calculated voltages are used to update the conductivity distribution, then a new set of calculations is carried out and the reconstruction procedure is iteratively repeated.

The reconstruction process can be formally defined as the solution of the system $[F][\sigma]=[V_m-V_c]$. This is a non-linear system, because the elements of matrix [F] are not constant but they are strongly dependent on the conductivity distribution $[\sigma]$. Thus, in order to solve this system it must be linearized (directly or indirectly) around an initial estimate $[\sigma]^o$, e.g. by expanding in Taylor series and keeping only the linear terms, solve the resulting linear system, update the conductivity to a better estimate $[\sigma]^1$ and iterative repeat this procedure.

Furthermore, after linearization the resulting matrix is again ill-posed, (e.g. [6, 17, 18]). From a physical point of view, the current flow tends to follow the highest conductivity path. Thus, when the conductivity of an area is changed the current streamlines are redistributed so that the effects of this change are minimized. This means that fairly large conductivity changes may result in very small changes in the surface voltages, [16]. In the converse manner, small errors in either the measured (V_m) or calculated (V_c) surface voltages may be translated into large errors in the estimated conductivities. This is the fact causing the ill-posedness in conductivity imaging and

constituting a limit in both its resolution and accuracy. Moreover, this problem is strongly dependent on the data collection scheme employed, namely the relative positions of the driven electrodes. For adjacent driven electrodes rotated/moved about the surface, the surface voltages are less sensitive to the central volume, while for an increasing electrodes relative distance the surface voltages become more sensitive to the central volume and less sensitive to the volume near the surface. The best data collection would be the one giving the same and as high as possible sensitivity over the whole volume, this would result to the best possible conditioning of matrix [F]. An optimum driven electrode distance, but for the 2-D imaging, has been proposed by Kyriacou et al [12] based on the above approach.

Mathematically, the ill-conditioning is reflected on matrix [F] where the ratio of the maximum over minimum eigenvalue is a measure of its ill-posedness. As it is expected, but also proved by Yorkey et al [6], the maximum eigenvalue is related to the area with highest sensitivity, while the minimum one is related to the area with lowest sensitivity. For the 2-D case and adjacent driven electrodes a ratio of max/min eigenvalue of the order of 10^6 was found, [6]. The ill-conditioning effects are stronger for the 2-D model (current is forced to flow in a plane), while a 3-D model improves the conditioning of the problem.

Another effect pointed out from the early steps of EIT, [19], is that the image reconstructed with 2-D algorithms is contaminated by structures above and below the active electrodes plane. This due to the fact that measurements are carried out on a real (3-D) object, where of course the equipotentials extend into the third dimension as well. This results in a distortion of the image toward the center and it has been observed by all EIT researchers at their attempt to reconstruct static images from measurements on laboratory phantoms. Where-ever they put a single test anomaly it appeared in the center of the reconstructed image. This can be removed in general by "dynamic imaging techniques", e.g. reconstructing also the image of a homogeneous tank and subtracting it from the image received with the anomaly. An alternative technique in our previous 2-D studies [20] is to measure on a tank with (let them V_{m1}) and without anomalies (let them V_{m2}), subtract the two sets and use the difference (V_{m1}-V_{m2}) in the reconstruction process. This technique efficiently handled the above problem and gave good results (correct offset position and satisfactorily good conductivity). A more definite solution without the homogeneous tank measurements is expected by the employment of the 3-D

algorithms, since the 3-D FEM model accounts for the current flow (extensions of equipotentials) in all three dimensions.

In order for this paper to be self sustained let us first briefly describe the 2-D modified perturbation method (2D-MPM) before moving on to the 3D-MPM. The 2D-MPM [12], is actually a modification of the "perturbation" method proposed by Kim et al [21] and improved by Yorkey et al [22]. They used constant voltage driven electrodes and measured the exiting currents. The perturbation method is based on the "sensitivity matrix" defined as the change of the measured current (ΔI) versus a change in an elements resistivity ($\Delta\rho$), namely $\Delta I/\Delta\rho$. Even though notified in [22], that this matrix is non-linear (likewise each $\Delta I/\Delta\rho$) they changed the resistivity by a factor of ten (from 100 to 1000Ω•cm) to calculate ΔI. So, they changed the resistivity of each FEM element in turn and they solved Laplace equation to calculate ΔI at each "measuring" electrode. This is of course a very time consuming procedure, especially if the non-linear sensitivity matrix is to be calculated at each EIT iteration using a small perturbation $\Delta\rho$ for more accurate calculations. Kyriacou et al [12] stated that instead of using $\Delta I/\Delta\rho$, which is a linear approximation of the derivative $\partial I/\partial\rho$, it is better to use the derivative itself. Also, since it has already been established that is better to inject current and measure voltages at pairs of electrodes (ports), then the partial derivatives $\partial I/\partial\rho$ or $\partial I/\partial\sigma$ should be used. The matrix defined by the partial derivative of the voltage difference observed at a port-i with respect to the conductivity of the jth FEM element, and for every combination i, j is called "Jacobian matrix", $J_{ij}=\partial V_i/\partial\sigma_j$. The MPM reconstruction algorithm is then given in the form :

$$\acute{o}_j^{\,n} = \acute{o}_j^{\,n-1} + k\,\frac{\sum_{i=1}^{M} \frac{V_{mi} - V_{ci}}{V_{mi}} \frac{\partial V_i}{\partial \acute{o}_j}}{\sum_{k=1}^{M} \left| \frac{\partial V_k}{\partial \acute{o}_j} \right|}\ \acute{o}_j^{\,n-1} \qquad (13)$$

where the superscript n denotes the iteration and M is the total number of linearly independent measurements from all projection angles (driven electrodes combinations). V_{mi} and V_{ci} are the measured and calculated voltages at the ith sensing port. k is a relaxation factor. Until now we have set k=1, since a higher or lower value does not seems to improve convergence. But further investigation is needed to estimate the effects of k.

Exactly the same formulae (13) can be used for a 3-D conductivity reconstruction, but the voltages V_{mi}, V_{ci} and the derivatives $\partial V_i/\partial\sigma_j$ must be calculated from a 3-D FEM model, σ_j representing the conductivity of the jth volume element.

There is some theoretical evidence that it is better to reconstruct the resistivity (ρ) instead of conductivity (σ) when constant current (I) is injected and the surface voltage (V_m) is measured/calculated. This is simply based on the definition of the impedance $Z=V_m/I$ and the proportionality $Z\propto\rho$ or $Z\propto 1/\sigma$.

Namely, the resistivity is linearly proportional to the measured voltage $\rho\propto V_m$, but the conductivity is inversely proportional to V_m as $\sigma\propto 1/V_m$. From a first sight it is then truly reasonable to reconstruct resistivity. But, recalling that the problem is non-linear and is always somehow linearized around a guess $\rho^{(n)}$ or $\sigma^{(n)}$ which after the solution is updated by a small amount $\Delta\rho$ or $\Delta\sigma$ as $\rho^{(n+1)} = \rho^{(n)}+\Delta\rho$ or $\sigma^{(n+1)} = \sigma^{(n)}+\Delta\sigma$, it is then expected that no serious improvement will be obtained by reconstructing ρ instead of σ. In other words, moving along a curve of the form y=a/x in small linear steps seems to be as easy as along a curve y=bx. What remains to be proved, is the convergence rate when imaging ρ or σ. It seems that when the initial guess is far away from the true one then σ-imaging would offer faster convergence, but as we get closer ρ-imaging could perform better. This could lead to a reconstruction strategy like, starting with σ-imaging and after some iterations turn to ρ-imaging. Nevertheless, the reconstruction formulae for ρ-imaging is formally the same as given in Eq.(13), just substituting σ for ρ and of course calculating derivatives with respect to ρ. It is then :

$$\tilde{n}_j^n = \tilde{n}_j^{n-1} + k\,\frac{\sum_{i=1}^{M}\frac{V_{mi}-V_{ci}}{V_{mi}}\frac{\partial V_i}{\partial\tilde{n}_j}}{\sum_{k=1}^{M}\left|\frac{\partial V_k}{\partial\tilde{n}_j}\right|}\,\tilde{n}_j^{n-1} \tag{14}$$

Let us at this point make a step forth and back to explain why the MPM algorithm for ρ- and σ- imaging are quite the same (this is not true for all EIT algorithms). The derivatives $\partial V_i/\partial\sigma_j$ and $\partial V_i/\partial\rho_j$ involved in Eqs.(13) and (14) are given later in Eqs.(18) and (19). They differ only by a term $(1/\rho_j^2)$ occurring in both the numerator and denominator of Eq.(14) and thus eliminated, as well as a minus sign which is also eliminated by a sign change in the difference (V_{mi} - V_{ci}). Concerning the convergence

criteria, there may be two cases. First the practical imaging case, when only the available information can be considered, and second the trial testing of the algorithm with computer or laboratory phantoms, when the target model conductivity vector σ_{true} is also known. A measure of the available information can be defined by the mean squared voltage differences (SSQ) between the measured (V_m) and the calculated (V_c) vectors at each iteration. Usually the division by the number of elements (P) is omitted (but when comparing imaging of different models it must be used), so we have :

$$SSQ = \sum_{i=1}^{M} \left(V_{mi} - V_{ci}\right)^2 \tag{15}$$

The rate of convergence can be defined in any case be the rate of decreasing SSQ versus the number of iterations. The reconstruction will stop whenever SSQ approaches the measurements/calculations error or when SSQ starts to increase (divergence). The actual error is always that of the conductivity (σ-error), but since the target distribution is unknown in practice, this can only be used for comparing different reconstruction algorithms or phantoms. This is defined by Yorkey et al [6], as :

$$\sigma\text{-error} = \frac{\sum_{i=1}^{P} (\sigma_{true}^{i} - \sigma_{calc}^{i})^2}{\sum_{i=1}^{P} (\sigma_{true}^{i} - \bar{\sigma}_{true})^2} \tag{16}$$

where $\bar{\sigma}_{true}$ is the average value of the target conductivity profile.

4. EVALUATION OF JACOBIAN MATRIX

The Jacobian matrix entries are calculated from closed form expressions based on an equivalent resistor network of each FEM element, the network compensation theorem and the element nodal voltages. It must be pointed out that these calculations are very fast, since all the quantities are already available. Especially, the nodal voltages are already calculated during the solutions of Laplace equation for every projection angle needed in any case to calculate the sensing ports voltages V_{ci} involved in Eq.(13). Yorkey et al [6] examined the compensation as well as a "standard" technique for the calculation of the Jacobian for a 2-D rectangular mesh model. In our case we decided to use the compensation theorem technique because it can be easily extended to the 3-D case and it is a clarified one. The standard method on the other hand involves additional derivatives

(they can be performed analytically) as well as the inverse of the FEM master matrix [Y]. Thus the standard method is more compatible with algorithms using a direct technique to solve the FEM system of equations.

The equivalent resistor network of an arbitrary (jth) parallelepiped element is shown in Fig.3b. It is consisted of 28 conductances (Y_{mn}) connecting the element vertices. Their values are given by the non-diagonal coefficients of the parallelepiped element matrix $[Y]^e$ given in Eq.(10). The symmetric form of $[Y]^e$ is also an indication that it can be represented by a resistor network, while its diagonal elements can be considered as "self conductances" and do not contribute to the voltages changes. Let the conductances of Fig.3b to the locally numbered as ℓ=1 to 28 and their value written as $Y_{mn}=Y_\ell=S_\ell\sigma_j$, with S_ℓ being the geometrical weight constants.

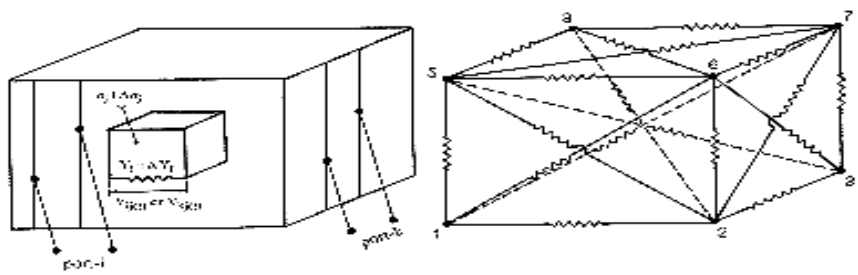

a b

Figure 3. a) Definition of ports-i and -k and perturbation of element conductivity from σ_j to $\sigma_j+\Delta\sigma_j$. and b) Equivalent resistor network of a parallelepiped element.

Consider two of the ports as -i and -k defined in the 3-D model sketch of Fig.3a and Y_ℓ an arbitrary conductance of the jth element. During the Laplace solutions for the calculated surface voltages ($[V_c]$) a constant current I_i is applied at the ith port and the potential distribution is obtained, so the voltage $V_{ij(\ell)}$ developed across the conductance Y_ℓ can be readily estimated. Similarly let this voltage be $V'_{kj(\ell)}$ when an equal current $I_k=I_i=I$ is applied at port-k but with the conductivity of the ith element perturbed to $\sigma_j+\Delta\sigma_j$, or the ℓth conductance perturbed to $Y_\ell+\Delta Y_\ell$. Considering for a moment only the perturbation of the conductance Y_ℓ, then the geometry is in principle the same with that used by Yorkey et al [6] to derive the derivative $\partial V_i/\partial\sigma_j$. They employed the compensation principle of electric circuits in conjunction with the discrete form of Geselowitz sensitivity theorem [23] given by Murai and Kagawa [24] and Nakayama et al [25].

According to this approach, the voltage change Δv_i at port-i when a current I is applied at port-k and the conductance Y_ℓ is perturbed to $Y_\ell + \Delta Y_\ell$ is :

$$\Delta V_{ij(\ell)} = -(\Delta Y_\ell / I)\, V_{ij(\ell)}\, V'_{kj(\ell)} \tag{17}$$

Assuming a differential perturbation $\Delta\sigma_j \rightarrow \partial\sigma_j$ which gives $\Delta Y_\ell \rightarrow \partial Y_\ell = S_\ell \partial\sigma_j$, then the voltage across $Y_\ell + \Delta Y_\ell$ would be practically equal to that without perturbation, or $V'_{kj(\ell)} = V_{kj(\ell)}$. Also, when σ_j is perturbed, then all the 28 element conductances are also perturbed. Thus, the resulting voltage change at port-i is simply estimated by summing Eq.(17) over all the element conductances, as $\Delta V_i = \sum_\ell \Delta V_{i(\ell)}$. Rearranging this summation the J_{ij} component of the Jacobian is obtained as :

$$J_{ij}(\acute{o}_j) = \frac{\partial V_i}{\partial \acute{o}_j} = -\frac{1}{I} \sum_{\ell=1}^{28} S_\ell\, V_{ij(\ell)} \cdot V_{kj(\ell)} \tag{18}$$

The derivatives with respect to resistivity are readily obtained from (18) by just substituting $\sigma_j = 1/\rho_j$, which gives :

$$J_{ij}(\tilde{n}_j) = \frac{\partial V_i}{\partial \acute{o}_j} = \frac{1}{I\tilde{n}_j^2} \sum_{\ell=1}^{28} S_\ell\, V_{ij(\ell)} \cdot V_{kj(\ell)} \tag{19}$$

Actually, equations(18) and (19) are quite general and can be used for any FEM element by just substituting with its specific constants S_ℓ.

5. DATA COLLECTION SCHEME-LINEARLY INDEPENDENT MEASUREMENTS

The data collection scheme seems to be the most serious problem in 3-D EIT imaging. First, every EIT specific application puts some constraints to the electrodes placement. In geophysical applications electrodes can be placed only on the top surface, while medical applications, in which we are interested herein, restrict the electrodes placement on the lateral body surface. Until now there is not (or at least we are not aware) any work studying the optimum position of electrodes in 3-D geometries, handy electrode positions maximizing the EIT sensitivity. A simplified approach is to handle separately a horizontal and a vertical cross-section. Let us explain this with an example. A three layers model is shown in Fig.4 with each layer divided into 8x8 elements.

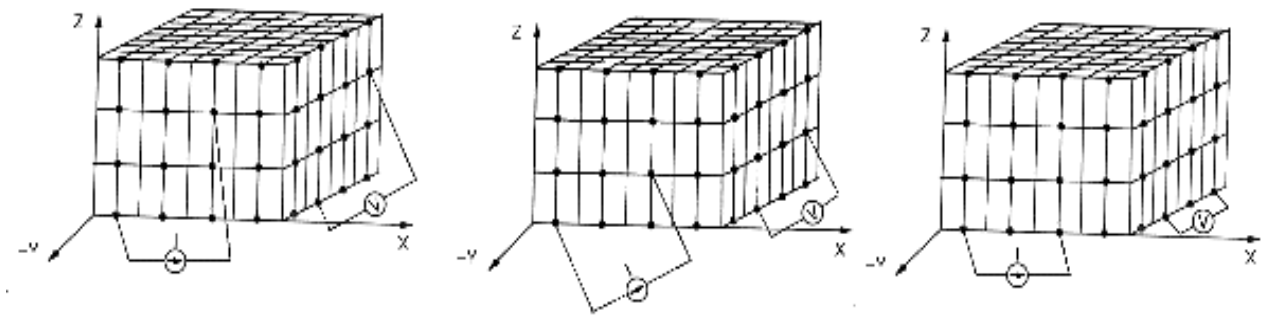

a b c

Fig.4. Data collection schemes or selection of projection angles. a) Diagonal electrodes with large distance, b) Nearby diagonal electrodes and c) coplanar electrodes.

Two possible diagonal driven electrode pairs (excitation ports) are shown in Fig.4a and 4b, while a coplanar one is shown in Fig.4c. Recall at this point, that the scheme described in the previous section for the calculation of the Jacobian matrix requires that the voltage sensing electrode pairs (measuring ports) must be defined exactly in the same manner as the excitation ports. Namely, define the virtual ports in the same manner all over the model, use one of them for excitation and all the others for measuring/calculating the voltages. Returning back to the data collection problem, it was found in [12] that for 16 electrodes (numbered successively) around an 8x8 element 2-D model the best projection angles (excitation ports selection) is in turn 1-3, 2-4, ... Thus, if coplanar electrode pairs should be used, then the best scheme would be that of Fig.4c. Using the same approach for a vertical cross-section where there are only four electrodes at each vertical side, the electrodes should have vertical distance of only one layer. In this sense the configuration shown in Fig.4b would be preferable than that of Fig.4a. Following this approach for a model with the same horizontal cross-section as that of Fig.4, but with eight layers (instead of three), we could say that the data collection scheme of Fig.4b is preferable. In order to define the linearly independent measurements needed in the reconstruction process we must first answer the following question. When we drive current across one layer, using for example the scheme defined in Fig.4b, do we make measurements/calculations across all the other layers? and even more important can we use the voltages measured across one layer to update the conductivity of all the other

layers including itself? For example, when injecting current at a port across the first layer, measurements made across the third layer can be used to update the conductivity of the first layer? and even most those of the second or any other layer? Logically, the answer to all these questions should be yes. This is because any possible complicated effects are taken into account during the calculation of the Jacobian matrix which defines the sensitivity of the specific voltage measuring port with respect to the conductivity of the element whenever this is in the 3-D domain. Also, this calculation depends or equivalently contains the information (voltage distribution) offered from the injection of a current at this specific measuring port as well. This generalized data collection scheme is not yet investigated and requires a lot of simulation work. Liu et al [9] studied a model with three layers each one with 4x4 elements giving a total of 48 unknown conductivities. They assumed N_1=8 point equispaced electrodes around the periphery of each one of the four layers. They used both adjacent coplanar and diagonal data collection schemes but with adjacent electrodes as shown in Fig.4b, 4c with the dotted lines. They assumed voltage measurements only around the layer to which they injected current, thus they updated a layer's conductivity only by measurements carried out around it. In other words they handled each layer separately. The linearly independent measurements in such a data collection can be defined by considering each layer as a 2-D model. So, for each layer of the model in [9], there are 7 unique projection angles and 8 measurements (including the one on current carrying electrodes) for each one, giving a total of 56 measurements. But, due to symmetry (V_{ij}=V_{ji}) only half of them are linearly independent, giving 28 unique voltage measurements per layer or 3x28=84 for the whole model. In general for N_1 electrodes placed around each level, there are $N_1(N_1-1)/2$ unique measurements per layer, e.g. [24]. In practice the four - electrodes technique, (two electrodes for injecting current and two separate electrodes for measuring voltage) for the data collection is now well established. Thus, avoiding voltage measurements on current carrying electrodes we have for the coplanar configuration $N_1(N_1-3)/2$ unique measurements, while for the diagonal configuration these remain $N_1(N_1-1)/2$.

In the case when voltage measurements are carried out at all the layers (let N_L= number of layers and N_L+1= number of levels) and N_1 electrodes are placed around each level, there are $N_L N_1$ possible projection angles for the diagonal and $N_L(N_1-1)$ measurements for each one of them. The total number of unique measurements is then $M= N_L^2\ N_1(N_1-1)/2$. For the model studied in [9] it is then M=252 (instead of 84), while

for the model shown in Fig.3 with N_L=3, N_1=16 and 3x8x8=192 unknown conductivities we have M=1080 unique measurements.

Finally, it must be noted that the number of unique measurements, which depends on the total number of electrodes ($N_L N_1$), restricts the number of the unknown conductivities (P), namely the number of elements into which the FEM model is to be subdivided. Moreover, an over-determined problem is inevitable in order to satisfactorily handled the measurements -calculations inaccuracies. For the 2-D problem a limit of the order of P<M/2 is recommended, while a good limit for 3-D seems to be P<M/4. This limit turns out to put a limit on the spatial resolution, since the relative distance between neighboring electrodes must be large enough so that the voltage between them is also large enough to be measured with the desired accuracy.

5. NUMERICAL RESULTS

A lot of 3-D computer phantoms are reconstructed in order to test the present algorithm. First, a vertically homogeneous model with 3 identical layers subdivided into 3x8x8=192 voxels, with 16 electrodes around each level as shown in Fig.4, was tried. The coplanar (Fig.4c) as well as the diagonal (Fig.4b) data collection scheme was used in turn. A homogeneous initial conductivity was assumed and the algorithm performed very well in both cases. The convergence curves are shown in Fig.5, namely the conductivity (σ-error) versus the number of iterations in Fig.5a and the voltage squared error (SSQ) in Fig.5b. The conductivity for one of the layers of the target model is shown in Fig.6a and for the reconstructed image at the 15th iteration in Fig.6b. The image obtained for the two other layers was almost identical as expected.

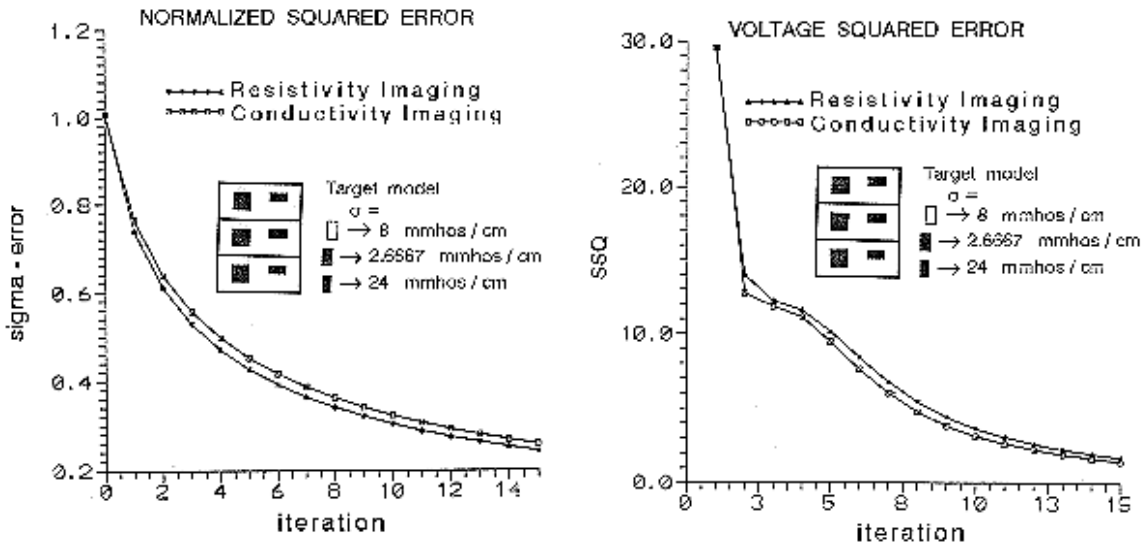

a b

Figure 5. Convergence rate of 3D-MPM for a vertically homogeneous 3-layers computer phantom, a)Conductivity error (σ-error), and b) Voltage squared error (SSQ) versus the number of iterations.

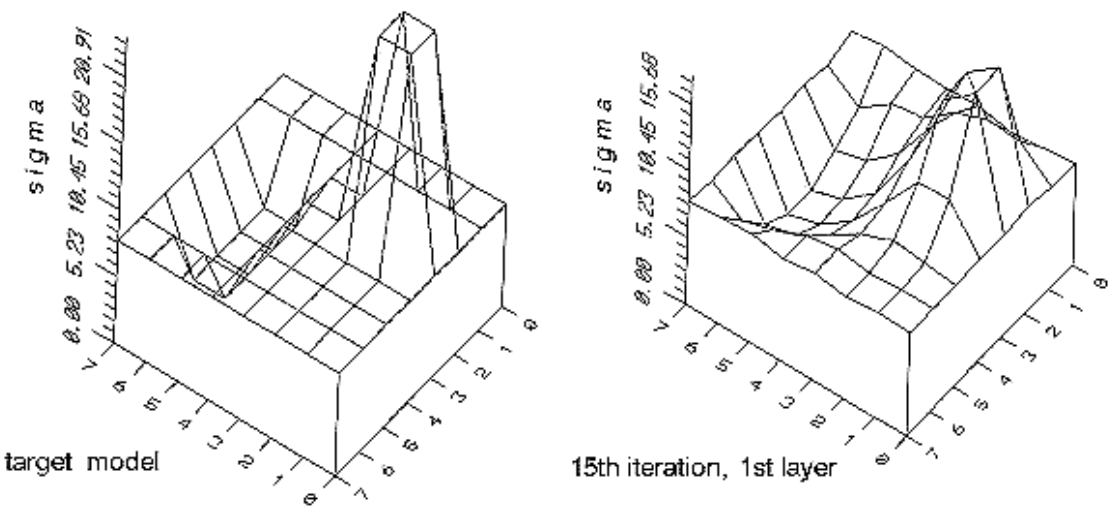

a b

Figure 6. Conductivity distribution for one of the layers of Fig.5. model, a) Target model and b) Reconstructed image at the 15th iteration.

A model like the previous one (shown in Fig.3), but with eight layers was then tried. It was considered a conductivity distribution with two anomalies (each one consisted of six elements), one at the 3rd layer with σ_1=2.667mmhos/cm and the other at the 6th layer with σ_2=2.667mmhos/cm, while the rest of the model is assumed homogeneous with σ=8.0mmhos/cm. A 3-D presentation for the two layers with the anomalies is shown in Fig.7., while the reconstructed images for each layer at the 2nd iteration are shown in

Fig.8. The first two layers (Fig.8.a,b) start to sense the lower anomaly which appears at the 3rd layer (Fig.8.c). From the 4th layer the higher anomaly starts to develop (Fig.8.d) and gets its peak value at the 6th layer (Fig.8.f) where it truly exist. At the two top layers the higher anomaly starts to decrease. One observes that in the reconstructed image, the anomalies are gradually developed from layer-to-layer but not abruptly. This is expected and has already noticed in the 2-D case, where a gradual change toward the anomaly occurred. Nevertheless, the position and the relative value has been approximately located, with their peak value appearing at the correct point.

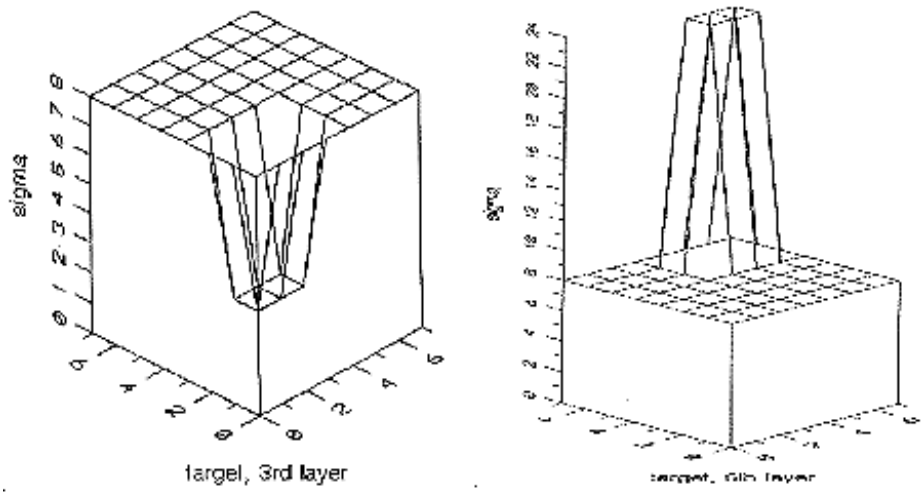

a b

Figure7. A vertically inhomogeneous target model. Only the conductivity of the 3rd and the 6th layers having anomalies are presented in a) and b) respectively.

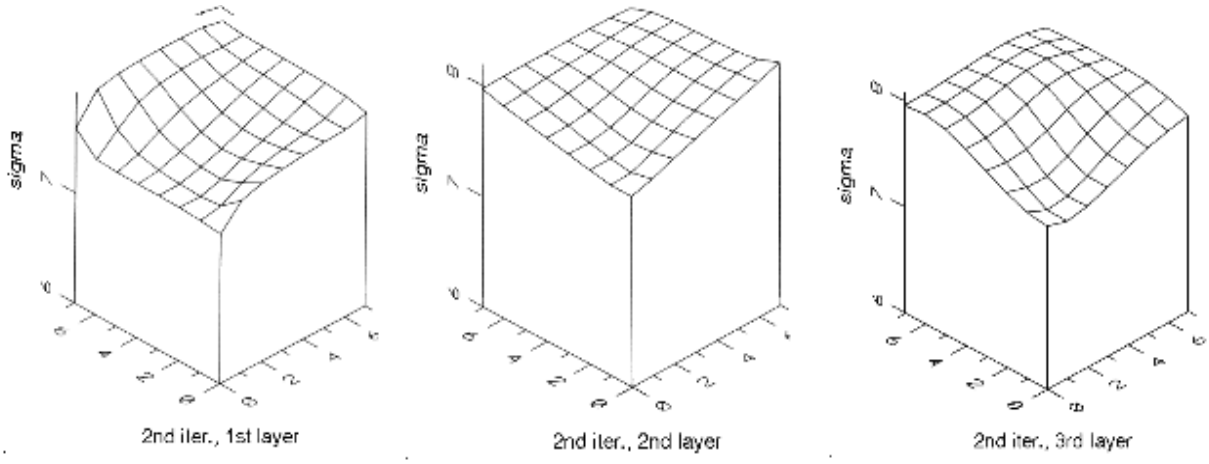

a b c

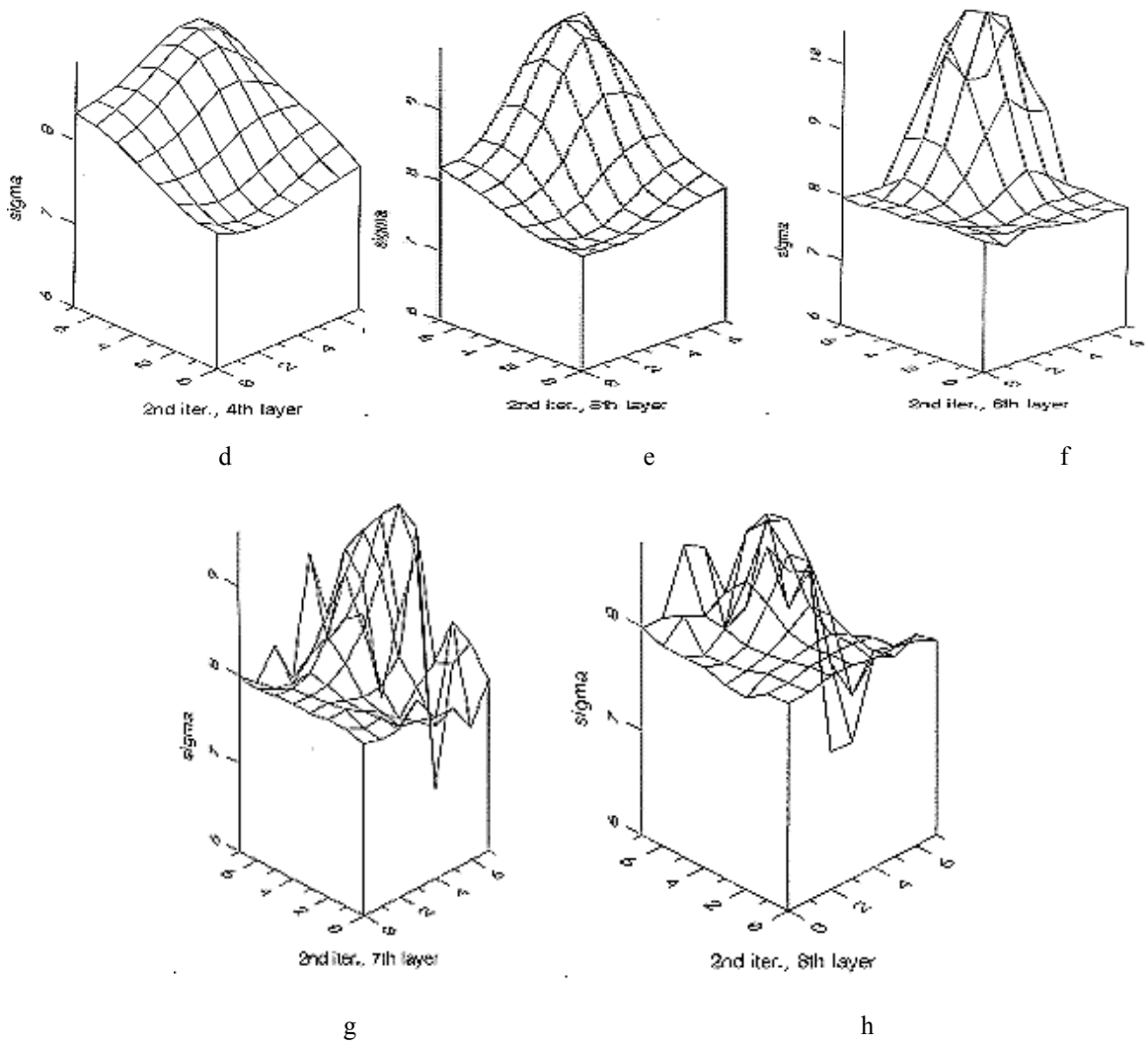

Figure 8. Reconstructed images for the model of Fig.6 at the 2nd iteration and for the 1st to 8th layers are presented in a) to h) respectively.

6. CONCLUSIONS

A reconstruction algorithm for 3-D EIT is developed based on the extension of the modified perturbation method. For this purpose the forward problem solution and the calculation of the Jacobian matrix were performed in a 3-D space. Some data collection schemes were examined, but this problem turns out to be vital in 3-D imaging and further investigation is needed. Finally, some successfully reconstructed 3-D computer phantoms are presented

REFERENCES

[1] D.C. Barber and B.H. Brown, “Applied potential tomography”, J. Phys. E. Sci. Instrum., Vol.17, pp.723-733, 1984.

[2] R.L. Parker, “The inverse problem of resistivity sounding”, Geophysics 42, pp.2143-2158, 1984.

[3] A. Wexler, B. Fry and M.R. Neumann, “Impedance Computed Tomography Algorithm and System”, Appl. Optics, Vol. 24, pp. 3985-3992, 1985.

[4] K.A. Dines and R.J. Lytle “Analysis of Electrical Conductivity Imaging”, Geophysics, Vol. 46, pp. 1025-1036, 1981.

[5] B.H. Brown, “Tissue Impedance Methods”, in “Imaging with non-ionizing radiations” edited by Daphne F. Jackson, Surrey Univ. Pres., 1983.

[6] T.J. Yorkey, J.G. Webster and W.J. Tompkins, “Comparing Reconstruction Algorithms for Electrical Impedance Tomography”, IEEE Trans., Biom. Eng., Vol. BME-34, pp. 843-852, Nov. 1987.

[7] A. Wexler, “Electrical impedance imaging in two and three dimensions”, Clin. Phys. and Physiol. Meas., vol.9, Suppl.A, pp.29-33, 1988.

[8] C.J. Kotre, “EIT image reconstruction using sensitivity weighted filtered backprosection”, Physiol. Meas. vol. 15, Suppl. A, pp.125-136, 1994.

[9] W.P. Liu, P. Hua and J.G. Webster, “Three dimensional reconstruction in electrical impedance tomography”, Clin. Phys. Physiol. Meas. vol. 9, Suppl. A, pp. 131-135, 1988.

[10] J. Goble and D. Isaacson, “Optimal current patterns for three-dimensional computed tomography”, Proc. Annual Int. Conf. IEEE Eng. in Medicine and Biology Soc., vol. 11., pp. 463-464, 1989.

[11] G.A. Kyriacou, C.S. Koukourlis, S. Mysteropoulos, C. Batas and J.N. Sahalos, “The modified Perturbation method in three dimensional EIT reconstruction”, 5th European Concerted Action in Impedance Tomography, Barcelona, Sept. 23-25, 1993.

[12] G.A. Kyriacou, C.S. Koukourlis and J.N. Sahalos, “A reconstruction algorithm of electrical impedance tomography with optimal configuration of the driven electrodes”, IEEE Trans. on Medical Imaging MI-12, no.3, pp.430-438, Sept. 1993.

[13] Y. Kim, “A three dimensional modifiable computer body model and its applications”, PhD Thesis, Dept. of Electr. and Comput. Engineering, University of Wisconsin, Madison, 1982.

[14] Webster J.G., editor, "Electrical Impedance Tomography", published by Adam Hilger imprint by IOP publishing, Bristol and New York, 1990.

[15] J.N. Sahalos, G.A. Kyriacou and E. Vafiadis, "An efficient finite element algorithm for 3D layered complex structures", Physiol. Meas. vol. 15, Suppl. 2A, pp. 65-68, 1994.

[16] D.B. Jorgenson, D.R. Haynor, G.H. Bardy and Y. Kim, "Computational studies and transvenous defibrilation in a detailed 3-D human thorax model", IEEE Trans., Biom. Eng., Vol. BME-42, pp. 172-184, 1995.

[17] D.C. Barber, “An overview of image reconstruction”, chapt. 4 in “Clinical and Physiological applications of electrical impedance tomography”, edited by D.Holder, University College London, UCL Press, 1993.

[18] W. Breckon and M. Pidcock, “Ill-posedness and non-linearity in electrical impedance tomography”, Proc. 20th conf. on information processing in Medical imaging, pp.235-244, Utrecht, Netherlands, June 1987.

[19] D.C. Barber, B.H. Brown and J.L. Freeston “Imaging Spatial distributions of resistivity using applied potential tomography”, Elec. Lett., vol 19, pp. 933-935, 1983.

[21] Y. Kim, J.G. Webster and W.J. Tompkins, “Electrical Impedance Imaging of the Thorax”, J. Microwave Power, Vol. 18, pp. 245-257, 1983.

[22] T.J. Yorkey, J.G. Webster and W.J. Tompkins, “An Improved Perturbation Technique for Electrical Impedance Imaging with some criticisms”, IEEE Trans., Biom. Eng., Vol. BME-34, pp. 898-901, Nov. 1987.

[23] D.B. Geselowitz, “An application of electrocardiographic lead theory to impedance plethysmography”, IEEE Trans., Biom. Eng., BME-18, pp. 38-41, 1971.

[24] T. Murai and Y. Kagawa “Electrical Impedance Computed Tomography based on a finite element model”, IEEE Trans., BME-32, pp. 177-184, 1985.

[25] K. Nakayama, W. Yagi and S. Yagi, “Fundamental study on electrical impedance CT algorithm utilizing sensitivity theorem on impedance plethysmography”, Proc. 5th Int. Conf. on Electrical Bio-impedance (ICEBI), pp.99-102, 1981.